Computational and Experimental Infrared Spectra of 1,4-Dinitropiperazine and Vibrational Mode Assignment

Suhithi M. Peiris,[†] Richard C. Mowrey,[‡] Craig A. Thompson,[†,§] and T. P. Russell*[,†]

Code 6112 and Code 6189, Chemistry Division, Naval Research Laboratory, Washington, D.C. 20375

Received: June 5, 2000; In Final Form: July 20, 2000

The IR spectra of both solid and matrix-isolated 1,4-dinitropiperazine (p-DNP) were obtained. The results indicate that 1,4-dinitropiperazine at 11 K is a mixture of three chair conformer structures and a single twisted-boat conformer. Vibrational modes of each conformer were computed using the B3LYP and BP86 density functional methods. The computed frequencies are used to assign vibrational mode symmetries to the spectra obtained experimentally. The conformer populations obtained by fitting experimental data with a weighted-sum spectrum generated from individual calculated conformer spectra were compared with calculated thermodynamic conformer populations at the experimental temperature. The energies of transition states between conformers were also calculated to clarify that the energy barriers to transformation between the three chair conformers are small enough to allow interconversion at the experimental temperature. Finally, calculated bond lengths and angles are compared to structural parameters obtained from single-crystal X-ray diffraction of p-DNP.

Introduction

1,4-Dinitropiperazine (DNP) or *p*-dinitropiperazine (p-DNP), also known as 1,4-dinitro-1,4-diazacyclohexane (DNDC), is one member of the nitramine (containing $N-NO_2$) family of energetic materials. In view of their utility both as plasticizers and as independent propellants, the thermal decomposition[1−5] and shock sensitivity[6] of many piperazine compositions with nitro, amine, and furazano, constituents have been previously investigated. In addition, computational studies using the Hartree−Fock self-consistent-field method have been reported on the structural and reactive properties of piperazine and its dinitro- derivatives.[7,8] These studies find the p-DNP structure with the ring atoms arranged in a "chair" form to have lower energy than the "boat" form. The three conformers of the chair form having nitro groups in equatorial−equatorial, equatorial−axial, or axial−axial orientations are reported to have very similar energies.

Previous experiments on the polarity of p-DNP solutions show a nonzero dipole moment.[9,10] A dipole moment may result in p-DNP, if either the ring structure is in boat form, or if the nitro groups are in different orientations (equatorial and axial) in the chair form. Therefore, two of the three chair conformers have dipole moments of zero, and only one chair conformer will contribute to polarity. The computational study which finds the chair form more stable explains that each chair conformer contributes to a dynamic equilibrium in solution yielding nonzero dipole moments.[7] However, the height of the energy barriers separating the conformers were not calculated in that study to confirm that interconversion can occur, nor were vibrational frequencies reported to aid the experimental investigation of existing p-DNP structures.

We studied p-DNP experimentally to investigate its structure using IR vibrational spectroscopy, and studied its crystalline solid to compare its structure to computed structural information. We also performed density functional method calculations to determine the structure and energy of each stable conformer of p-DNP and the energy barriers between these conformers. The vibrational frequencies for each stable structure were also calculated. We then use these calculated numbers to interpret our infrared experimental data and to evaluate the relative populations of the stable forms of this material under ambient conditions.

This is the first report of matrix-isolated infrared spectra obtained for p-DNP. Our spectra show a pattern of peaks more complicated than that resulting from the vibrations calculated for a single structure. Our B3LYP and BP86 calculations show that there are three minimum-energy conformers of the chair form and one minimum-energy twisted-boat conformer. All of these conformers have relative energies within 3 kcal/mol, confirming that p-DNP has several structures that are stable under ambient conditions. The calculations also show that the equatorial−equatorial (ee) orientation is the most stable conformer of the chair form, and add the information that the energy barriers to transition between the three chair conformers is only about 0.9 kcal/mol, enabling easy conversion between conformers at room temperature. In addition, the vibrational frequencies for each conformer were also calculated and compared with the experimental IR spectra to show that all three of the chair conformers (and possibly a small percent of the twisted-boat structure) are present in-matrix. The peaks in the experimental spectra were assigned vibrational modes by comparison with a weighted-sum spectrum generated from the calculated spectrum of each conformer. The weighted-sum conformer distribution was then compared to the calculated thermodynamic conformer populations, at the experimental temperature, showing good agreement. Finally, calculated bond lengths and angles are compared to structural parameters obtained from single-crystal X-ray diffraction of p-DNP.

[†] Code 6112.
[‡] Code 6189.
[§] NRC postdoctoral associate.

10.1021/jp002020t
Published on Web 09/01/2000

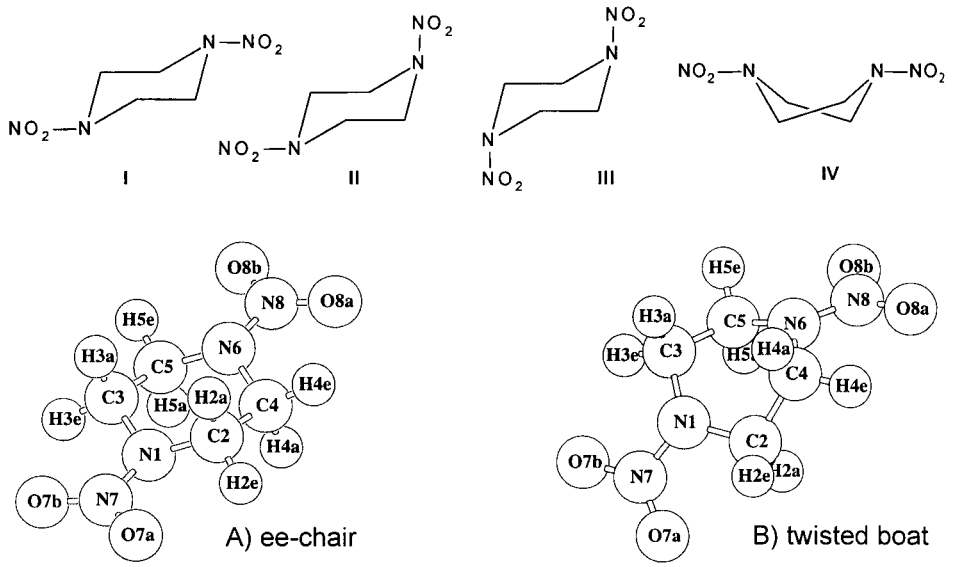

Figure 1. Three chair conformers and single twisted-boat conformer of p-DNP, the chair form as a ball-and-stick figure (including the numbering scheme for atoms in Table 4), and the twisted-boat form as a ball-and-stick figure.

Experimental Method

Samples of p-DNP were obtained from Dr. Cliff Bedford at China Lake, CA, and were used as received. Matrix-isolated samples of p-DNP were prepared in a vacuum chamber maintained at a background pressure of $\sim 1 \times 10^{-7}$ Torr. P-DNP was thermally evaporated from a resistively heated Knudsen cell at a temperature range between 30 and 85 °C. Temperature was maintained using an Omega 76133 temperature controller. A 250 mm orifice was required for the cap of the Knudsen cell. An argon gas spray (NG Industries, 99.999%) adjacent to the Knudsen cell was used to transport and deposit the sample on the cold window.

Matrix samples were collected on a CsI salt window maintained at 15 K by an Air Products, DE-202, closed cycle helium refrigerator. Deposition times ranged from 2 to 3 h at a Knudsen cell temperature of 85 °C. Under these conditions, the optimal argon flow rate was 2 mmol/h. Samples were analyzed using a Nicolet 740 infrared spectrometer with a MCT-A detector. For each sample, 256 spectra were averaged yielding a spectrum with 0.1 cm^{-1} accuracy and 0.5 cm^{-1} resolution.

Quantum Chemical Calculations

The structures corresponding to the lowest energy conformers of p-DNP and the transition states connecting them were computed using two density functional methods. The BP86 method uses Becke's 88 exchange functional[11] with Perdew's 86 correlation functional.[12] The B3LYP method combines Becke's three-parameter hybrid method[13] with the Lee−Yang−Parr functional.[14] The calculations used the Gaussian 98[15] quantum chemistry package. The 6-31G** basis set of Pople et al.[16] with pure "d" polarization functions was used. Harmonic frequencies were calculated using the forces calculated analytically from the second derivatives of the energy with respect to the nuclear coordinates. The vibrational frequencies computed by the B3LYP and BP86 methods are scaled by a factor of 0.9614 and 0.9914, respectively, to correct for systematic errors in the calculations.[17]

Results and Discussion

The two basic structures of p-DNP are the chair and the boat forms. The geometries of four different chair and boat structures were previously calculated with HF SCF,[7,8] but the vibrational frequencies for all identified conformers were not determined to assess whether the structures were local minima on the potential energy surface. Both HF and density functional methods were used to identify the stable p-DNP structures giving the same results on conformer stability. However, only results from the density functional calculations are presented here. Our density functional calculations indicate that the three conformers of the chair form (with nitro groups in the equatorial−equatorial (ee), equatorial−axial (ea) and axial−axial (aa) positions) are all stable structures, with real vibrational frequencies. However the boat form, while being a stationary point on the potential energy surface, has two negative frequencies and is not a stable structure. Following the eigenvectors for motion in coordinate space corresponding to these negative frequencies leads to the equatorial−axial chair conformer and a new p-DNP twisted-boat conformer. The new twisted-boat form is a stable structure with only real vibrational frequencies. We investigated several twisted-boat conformers but only one stable twisted-boat conformer, with the nitro groups approximately in the ee position, was found (equatorial and axial positions of the twisted boat cannot be clearly defined as there is no planar ring associated with this structure.). Attempts to locate stable twisted-boat structures with the nitro groups in the ea and aa orientations were unsuccessful. The molecule relaxed to the ee orientation for each initial structure tested.

The three stable chair conformers and the single stable twisted-boat conformer of 1,4-dinitropiperazine are shown in Figure 1. The conformers are numbered: I, chair with both NO_2 groups equatorial; II, chair with one NO_2 equatorial and one axial; III, chair with both NO_2 groups axial, to the plane formed by the four carbon atoms, and IV, twisted-boat with both NO_2 groups "equatorial". The chair form and the twisted-boat form are also shown as ball-and-stick figures. The minimum structural energy calculated (denoted E_{min}) and the total energy with the zero-point vibrational energy added (denoted $E_{tot,0K}$), for each conformer using the B3LYP and BP86 density functional methods are listed in Table 1. The $E_{tot,0K}$ energies for the three chair conformers are within 1 kcal/mol of each other. Therefore, if the barriers to transformation between conformers are small, p-DNP at ambient conditions will consist of mixtures of the conformers, with each conformer in kinetic equilibrium with

TABLE 1: Calculated Energies, Relative Energies, and Populations for the Three Chair Conformers, the Single Conformer of the Twisted-Boat Form, and the Transition States Connecting the Conformers

	BP86					B3LYP				
conformer	E_{min} + 676 (Hartrees)	δE_{min} [a] (kcal/mol)	$E_{tot,0K}$ + 676 [b] (Hartrees)	$\Delta E_{tot,0K}$ [b] (kcal/mol)	$\Delta G°$ [c] (kcal/mol)	rel abundance (%)	E_{min} + 676 (Hartrees)	ΔE_{min} [a] (kcal/mol)	$E_{tot,0K}$ + 676 [b] (Hartrees)	$\Delta E_{tot,0K}$ [b] (kcal/mol)	$\Delta G°$ [c] (kcal/mol)	rel abundance (%)
aa	−0.960259	0.0	−0.812386	0.194	0.616	20	−0.907762	0.541	−0.754394	0.832	0.992	11
aa* TS	−0.958515	1.094	−0.810968	1.084			−0.906122	1.570	−0.753116	1.63		
ea	−0.960131	0.0803	−0.812446	0.156	0.0	48	−0.908181	0.278	−0.754999	0.452	0.0	44
ee* TS	−0.958341	1.204	−0.811065	1.023			−0.906440	1.370	−0.753701	1.27		
ee	−0.960125	0.0841	−0.812695	0.0	0.303	31	−0.908624	0.0	−0.755720	0.0	0.00377	43
twist* TS	−0.948724	7.238	−0.801617	6.951			−0.897459	7.006	−0.744865	6.81		
twisted	−0.955563	2.947	−0.808000	2.946	2.80	1	−0.903851	2.995	−0.750965	2.98	2.25	2

[a] The energy of the conformers relative to the lowest energy conformer. [b] Includes the zero-point vibrational energy. [c] Calculated at 358 K.

the other two conformers. Hence Table 1 also includes the total energies ($E_{tot,0K}$) of the transition states between conformers. The transition state energies connecting the three chair conformers are all within 1−2 kcal/mol of the conformer energies. These energy barriers to transition between chair conformers are small enough for each conformer's nitro group to flip between equatorial and axial positions quite easily at room temperature, resulting in a dynamic equilibrium between the structures.

Now consider the twisted-boat conformer. Its $E_{Tot,0K}$ energy is also within 3 kcal/mol of the chair conformers, however its barrier to transition is slightly higher at 6−7 kcal/mol. Therefore, while this structure is stable and could exist in equilibrium with the chair conformers, its high energy relative to the chair conformers and high interconversion barrier indicate that it would be present as only a very small percent of the p-DNP at ambient conditions.

Figure 2 shows the same information presented as an energy diagram. Comparing E_{min} (energies without zero-point energy) (Figure 2A,C) the B3LYP method predicts the ee conformer of the chair form to be the most stable while the aa conformer is most stable when the BP86 method is used. However, when the zero-point vibrational energy is added to yield the total energy $E_{tot,0K}$ (Figure 2B,D), the ee conformer turns out to be the most stable chair conformer with both DFT methods. Both methods predict that the zero-point vibrational energy of the chair molecule increases as a nitro group moves from an equatorial to the axial orientation. Thus, the aa conformer has the largest zero-point vibrational energy of the three chair conformers. This is due to a general trend in which the vibrational frequencies for individual modes gradually increase in going from the ee to the ea and aa conformers. For example, looking at Tables 2 and 3, we see the frequencies of the CH_2 stretch modes increase, in general, in going from the ee to the ea and aa conformers. The frequencies of some modes (e.g., the Bu CH_2 bend mode) decrease but the overall trend is an increase in frequency. Previous theoretical calculations[7] using the HF−SCF method indicated that the aa orientation is the most stable structure, a result that differs from that predicted by the DFT methods in the present study. However, these HF−SCF calculations neglected the effects of the zero-point vibrational energy and used a smaller basis set than used in the current study. We computed the energies of the three chair conformers using the HF−SCF method and the 6-31G** basis set used in our DFT calculations. Comparing the energies, as well as the energies with the zero-point vibrational energy included, indicates that the ee conformer is lowest in energy followed by the ea and aa conformers, which agrees with the DFT results. Because the energies for each of the chair conformers are so similar it is not surprising that different theoretical models predict differences in their relative ordering.

The B3LYP/6-31G** vibrational frequencies for each conformer are listed in Table 2, along with descriptions of the vibration of each mode. The BP86/6-31G** vibrational frequencies calculated for each conformer are listed in Table 3. To easily visualize calculated frequencies and intensities as real spectra, a Lorentzian peak shape was produced for each calculated frequency with an amplitude equal to the calculated intensity and a peak FWHM of 1 cm^{-1}. Thus, calculated spectra were generated for each conformer and compared with the experimentally obtained spectra. Figure 3, shows the spectra obtained by the B3LYP method for each conformer, along with the matrix-isolated spectrum. (The BP86 spectra show similar features.) The experimental spectrum contains more peaks than each spectrum of a single conformer and many features that

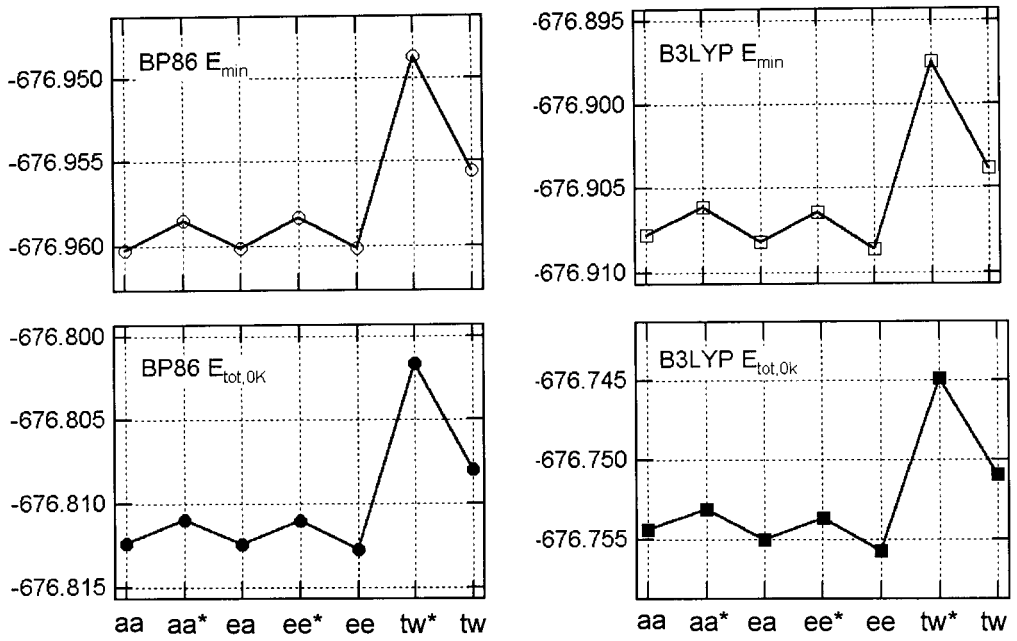

Figure 2. Calculated total energies of each conformer with ($E_{tot,0K}$) and without zero-point vibrational energy (E_{min}) using DFT with both BP86 and B3LYP methods.

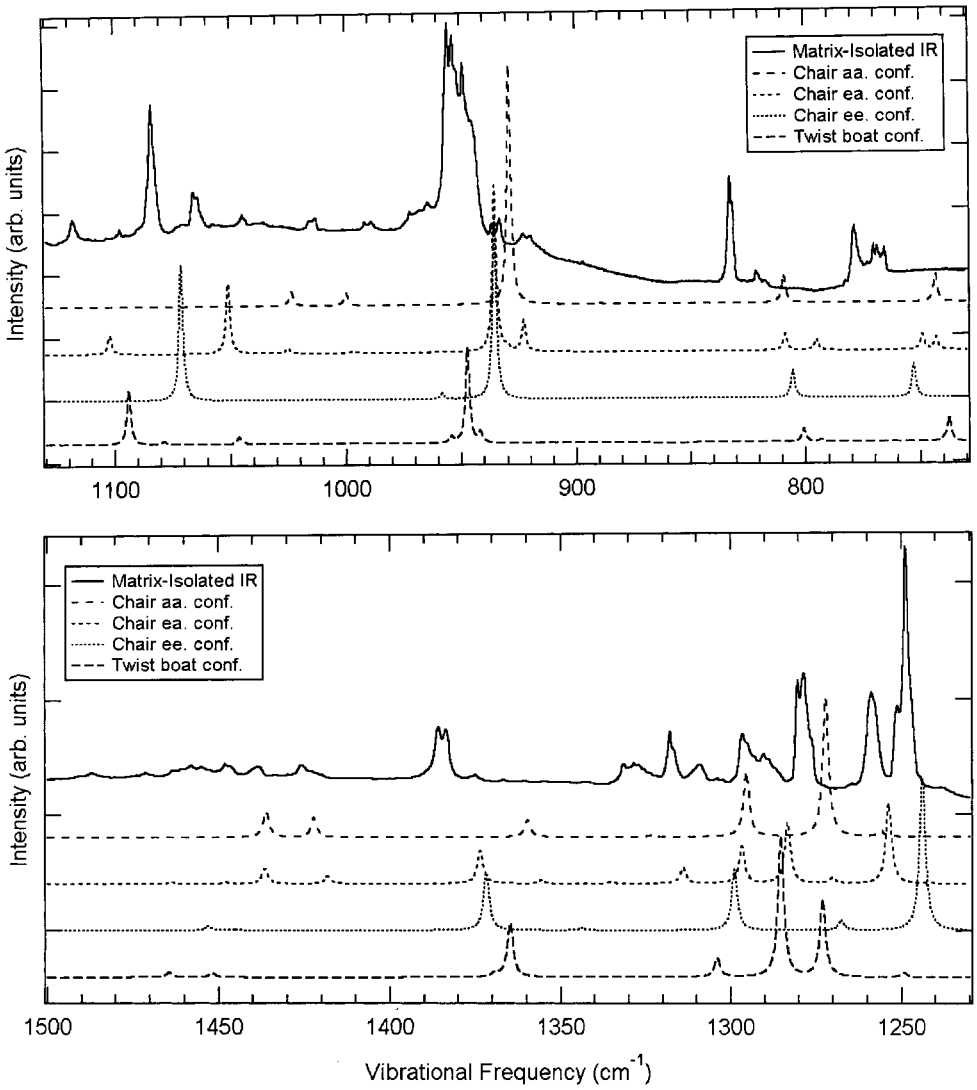

Figure 3. Calculated vibrational frequencies with Lorentzian peaks generated at each frequency for each conformer. Notice the matrix-isolated IR spectra has many more peaks (seemingly a sum of peaks from each conformer) than the spectrum of each individual conformer.

TABLE 2: B3LYP Calculated Frequencies, Symmetries, IR Intensities, and Description of Modes for the Four Stable Conformers

ee chair			ea chair			aa chair			ee twist-boat			
sym	freq	int	sym	freq	int	sym	freq	int	sym	freq	int	description
Bu	51.1	9.8	A′	46.2	6.1	Bu	55.2	9.8	A	23.7	8.2	NO_2−ring-NO_2 OOP bend
Au	80.2	0.02	A″	80.9	0.4	Au	80.7	0.031	B	67.5	4.2	NO_2−ring-NO_2 twist
Bg	104.5	0	A″	89.3	1.0	Ag	85.7	0	A	92.6	0.7	NO_2−ring-NO_2 twist
Ag	128.8	0	A′	114.2	2.8	Bg	94.6	0	B	132.7	0.7	N−C−C−N bends
Au	173.4	9.7	A″	167.1	4.5	Au	115.9	7.8	A	155.0	8.6	NO_2−ring-NO_2 bend
Bu	235.5	25.9	A′	267.1	13.4	Bg	360.4	0	B	219.4	11.1	ring twist
Au	247.5	0.62	A″	269.8	1.6	Ag	365.4	0	A	252.7	0.1	ring twist
Ag	275.2	0	A′	327.1	3.9	Bu	369.9	25.1	A	284.8	0.03	C−N−C bends
Bg	303.5	0	A″	375.9	0.9	Au	399.3	1.4	B	311.6	3.4	C−C−N−C−C ax twist
Ag	347.3	0	A′	425.7	12.7	Bg	426.3	0	A	335.1	2.6	C−N−C ax bend
Bg	461.0	0	A″	442.3	0.4	Ag	455.2	0	A	479.3	1.6	ring twist
Bu	484.2	9.6	A′	507.7	7.4	Bu	531.8	18.6	B	482.3	5.0	NO_2−ring-NO_2 sym str
Au	549.4	8.3	A″	553.6	9.0	Au	553.4	11.7	B	562.8	10.4	C−N−NO_2 eq bend
Bg	574.1	0	A″	584.7	3.6	Bu	591.9	5.3	A	587.5	2.3	C−N−NO_2 ax bend
Ag	637.4	0	A′	591.0	0.3	Ag	596.5	0	A	627.7	0.1	C−N−C ax bend
Bu	665.5	2.8	A′	649.6	2.0	Bg	604.1	0	B	641.0	3.0	C−C−N bends, C−N−C eq bend
Ag	747.5	0	A′	743.2	14.7	Ag	737.6	0	A	737.6	30.1	NO_2 ax OOP bend
Bu	753.0	40	A′	749.2	18.6	Bu	743.5	34	B	740.0	2.9	NO_2 eq OOP bend
Ag	802.0	0	A′	795.3	12.9	Ag	790.8	0	A	793.2	2.8	NO_2 eq bend, ring breathing
Bu	805.6	32.7	A″	806.8	0.1	Bg	795.2	0	B	800.9	16.6	C−C−N bends
Bg	831.8	0	A′	808.8	19.4	Bu	809.5	33.8	A	840.9	0.2	NO_2 ax bend, C−N−C bend
Bu	935.6	214.9	A′	922.8	36.8	Au	890.0	1.7	B	941.8	12.2	C−C str, C−N str
Ag	947.8	0	A″	930.1	5.3	Ag	898.8	0	B	947.4	113.5	C−C str
Au	958.5	7.9	A′	935.5	198.7	Bu	929.0	287.6	A	954.4	7.2	C−C str, C−N str
Ag	1024.0	0	A′	996.9	1.7	Ag	973.5	0	A	1044.9	2.5	C−C str
Au	1042.2	0.29	A″	1025.2	6.2	Au	1000.0	15.6	B	1046.4	7.7	CH_2 rock
Bu	1071.3	162.6	A′	1051.0	83.5	Bu	1023.6	17.3	A	1078.9	3.8	N−N str, C−N−C bend
Ag	1095.6	0	A′	1102.3	22.6	Ag	1111.0	0	B	1094.1	66.8	C−C, C−N str
Au	1132.3	6	A″	1135.0	0.9	Bg	1146.4	0	B	1165.1	11.4	C−C, C−N str
Bg	1182.2	0	A″	1170.4	8.9	Au	1147.3	1	A	1198.0	6.2	CH_2 twist
Bg	1232.3	0	A″	1226.3	1.6	Bg	1229.5	0	B	1223.1	107.8	C−N str
Bu	1243.8	494.8	A′	1253.7	257.1	Au	1256.1	20.5	A	1249.2	15.5	N−NO_2 eq str
Au	1267.6	32	A″	1270.1	18.2	Bu	1272.1	455.4	A	1269.2	2.5	C−N str
Ag	1284.3	0	A′	1283.3	195.4	Bu	1295.4	213.8	B	1273.1	249.4	N−N str, C−N str, NO_2 str
Ag	1294.1	0	A′	1296.7	118.8	Ag	1299.6	0	B	1285.3	451.7	N−N str, C−N str, NO_2 str
Bu	1298.9	194.4	A″	1302.8	1.3	Bg	1303.1	0	A	1304.0	61.7	CH_2 wag
Bg	1300.8	0	A′	1314.0	52.4	Ag	1305.5	0	A	1309.6	0.6	N−N ax str, C−C str
Au	1343.8	7.1	A″	1335.4	4.7	Au	1323.3	4.5	B	1349.8	1.8	C−C str, CH_2 wag
Bu	1371.8	185.3	A′	1355.8	10.3	Ag	1359.7	0	B	1364.8	174.6	NO_2 ax. sym str, CH_2 wag
Ag	1385.0	0	A′	1373.6	106.6	Bu	1359.7	56.3	A	1369.3	13.4	NO_2 eq. sym str, CH_2 wag
Bg	1440.4	0	A″	1418.2	25.0	Au	1422.2	64	B	1451.7	14.1	CH_2 bend
Au	1445.4	3.5	A′	1436.5	49.4	Bg	1422.9	0	B	1459.6	1.4	CH_2 bend
Bu	1452.9	13.3	A″	1447.6	4.6	Bu	1436.1	86.6	A	1464.3	15.8	CH_2 bend
Ag	1462.6	0	A′	1463.3	5.2	Ag	1443.3	0	A	1470.8	1.1	CH_2 bend
Au	1604.2	512	A″	1602.8	68.7	Bg	1597.2	0	B	1591.3	463.2	NO_2 ax, NO_2 eq asym str
Bg	1605.7	0	A″	1604.7	412.9	Au	1599.6	452.3	A	1592.5	45.8	NO_2 eq, NO_2 ax asym str
Au	2901.6	18.5	A″	2906.8	7.9	Au	2962.1	5.2	B	2928.6	15.9	CH_2 str
Ag	2903.9	0	A′	2908.9	26.3	Ag	2967.1	0	A	2933.9	2.1	CH_2 str
Bg	2912.6	0	A″	2968.7	3.0	Bg	2973.2	0	B	2943.7	5.3	CH_2 str
Bu	2915.4	86.5	A′	2974.3	32.3	Bu	2979.0	38	A	2946.9	49.6	CH_2 str
Au	3052.6	0.59	A″	3047.4	0.6	Bg	3063.0	0	B	3002.7	8.4	CH_2 str
Bg	3052.8	0	A′	3047.8	3.7	Ag	3063.0	0	A	3004.1	9.5	CH_2 str
Bu	3053.0	7.4	A″	3065.7	0.2	Au	3063.2	0.95	B	3045.6	7.9	CH_2 str
Ag	3053.1	0	A′	3065.9	0.8	Bu	3063.4	1.7	A	3046.1	0.4	CH_2 str

appear to be composed of multiple peaks from multiple conformers. This suggests that the matrix-isolated sample consists of more than a single p-DNP conformer. Initially, we compared combinations of two conformers in an attempt to reproduce the recorded spectrum. The combination spectrum was generated by adding the calculated spectra of two conformers (at a time, in various combinations) to generate spectra as though a 50% concentration of each conformer was in the IR matrix. We were unable to simulate all the peaks in the matrix-isolated spectra with the combinations of two calculated spectra. Next, combinations of the three chair conformers were considered. The spectrum generated using only the three-chair conformers did not completely describe the recorded spectrum either. The complete spectrum was reproduced when a spectrum with a weighted-sum of the calculated spectra of the three chair conformers and the twisted-boat conformer was generated. The "weight" assigned to each conformer was decided by the best (visual) simulation of experimental peaks throughout the IR data range. The best "simulation" was achieved by weighting the ee, ea, and aa chair conformers, and the twisted-boat in a 0.9:1:0.6:0.05 ratio. Figure 4 shows the simulated spectra from both the B3LYP and BP86 methods together with the experimentally obtained matrix-isolated spectrum of p-DNP. This ratio shows that p-DNP exists as a composition of structures, mainly of the chair form containing 35% of the ee conformer, about 39% of the ea conformer and 24% of the aa conformer, with a negligible contribution of 2% from the twisted-boat conformer.

We also identified the relative populations of conformer

TABLE 3: BP86 Calculated Frequencies, Symmetries, and IR Intensities, for the Four Stable Conformers, with Corresponding Experimentally Observed Frequencies and Observed Relative Intensities

ee chair			ea chair			aa chair			ee twist-boat			assignment from	expt
sym	freq	int	sym	freq	int	sym	freq	int	sym	freq	int	expt (cm^{-1})	intensity(%)
Bu	52.1	8.5	A′	46.4	5.4	Bu	54.3	8.8	A	27.2	6.6		
Au	82.5	0.02	A″	84.6	0.04	Au	83.7	0	B	79.0	4.7		
Bg	108.4	0	A″	93.3	0.96	Ag	84.3	0.03	A	94.4	0.4		
Ag	125.5	0	A′	112.2	2.4	Bg	99.8	0	B	133.6	0.8		
Au	171.4	9.1	A″	166.6	4.4	Au	114.0	6.9	A	176.7	9.0		
Bu	233.7	26.8	A′	267.7	1.2	Bg	355.8	0	B	230.9	9.9		
Au	251.0	0.24	A″	269.7	3.5	Ag	361.7	0	A	249.7	0.2		
Ag	271.5	0	A′	321.8	3.3	Bu	366.0	24.8	A	285.7	0.04		
Bg	297.9	0	A″	371.8	0.88	Au	392.2	1.7	B	330.5	4.9		
Ag	351.2	0	A′	420.7	13.1	Bg	423.1	0	A	349.5	3.7		
Bg	456.3	0	A″	439.4	0.15	Ag	446.7	0	A	472.3	2.5		
Bu	473.1	4.7	A′	495.4	7.2	Bu	514.5	24.1	B	480.8	2.0		
Au	547.0	6.1	A″	551.2	7	Au	548.4	9.3	B	559.4	7.9		
Bg	569.2	0	A″	578.8	2.6	Bu	583.8	4.8	A	583.9	2.3		
Ag	631.2	0	A′	580.5	0.13	Ag	586.1	0	A	623.9	0.003		
Bu	655.0	7.3	A′	641.8	4.8	Bg	601.9	0	B	632.9	1.1	689.9, 691.0	1, 1
Ag	730.1	0	A′	724.8	12.6	Ag	719.2	0	A	720.2	24.4	765.9	9
Bu	734.7	33.2	A′	730.7	15.2	Bu	722.9	26.1	B	723.2	2.5	768.9, 770.3, 778.6	2, 3, 6
Ag	796.0	41.6	A′	793.1	17.5	Ag	784.9	0	A	791.0	3.6	doublet 821.2	2
Bu	800.2	0	A″	800.3	0.3	Bg	788.4	0	B	793.2	21.9	doublet 832.6	18
Bg	827.8	0	A′	800.7	27.8	Bu	802.8	51.7	A	832.4	1.5		
Bu	919.6	251.2	A′	896.5	32.5	Au	879.3	0	B	928.6	140.0	920.3, 923.0, 933.4, 936.4	2, 2, 2, 1
Ag	921.7	0	A″	918.9	221.1	Ag	891.5	2.3	B	935.3	14.1	948.9, 953.4, 955.4, 964.3	32, 30, 31, 1
Au	951.4	10.2	A′	928.0	7.2	Bu	910.3	270.1	A	936.6	22.2		
Ag	1012.8	0	A′	986.7	0.6	Ag	958.5	0	A	1023.0	5.7	972.0	2
Au	1034.4	0.55	A″	1016.3	3.8	Au	990.1	9.4	B	1028.7	11.7	989.1, 1013.3, 1015.6	1, 2, 2
Bu	1052.1	119.2	A′	1032.2	53	Bu	1009.6	9.4	A	1061.4	3.3	1044.6, 1062.6, 1065.6	2, 3, 7
Ag	1082.4	0	A′	1087.7	22.4	Ag	1096.5	0	B	1075.3	44.7	1118.1	3
Au	1123.1	2.5	A″	1127.9	0.001	Bg	1143.3	1.8	B	1154.6	11.3	1128.8, 1140.8, 1142.9	2, 1, 2
Bg	1169.5	0	A″	1161.8	10	Au	1145.0	0	A	1188.3	10.0	1191.1	2
Bg	1226.2	558.9	A″	1221.7	0.53	Bg	1226.0	0	B	1207.5	100.1	1238.5, 1248.6	4, 79
Bu	1230.3	0	A′	1235.9	352.4	Au	1247.5	544.4	A	1238.5	19.2	1251.0, doublet 1258.5	41, 45
Au	1260.5	36.5	A″	1263.9	21.9	Bu	1250.8	26.1	A	1250.7	523.0	1278.7, 1280.0	55, 52
Ag	1261.1	0	A′	1265.5	66.8	Bu	1271.9	0	B	1256.0	0.8	1290.3	9
Ag	1277.7	0	A′	1266.4	106.5	Ag	1280.0	56.7	B	1269.4	28.6	1295.9	13
Bu	1279.4	69.8	A″	1284.8	2.4	Bg	1289.2	0	A	1270.3	70.9	1309.6	9
Bg	1280.1	0	A′	1303.0	34.2	Ag	1295.5	0	A	1294.4	0.9	1317.6	20
Au	1328.8	3.8	A″	1320.7	2.6	Au	1308.4	3.7	B	1332.6	1.0	1328.1, 1331.1	6, 9
Bu	1352.7	152.4	A′	1342.0	10.5	Ag	1325.6	0	B	1347.0	104.5	1375.4	3
Ag	1368.1	0	A′	1356.4	80.3	Bu	1348.6	47.8	A	1349.2	14.3	1383.8, 1385.6	23, 22
Bg	1430.9	0	A″	1404.0	29.6	Au	1406.9	71.1	B	1436.8	19.6	1425.3	5
Au	1435.0	4.5	A′	1422.0	46	Bg	1408.3	0	B	1450.7	1.7	1438.9	5
Bu	1442.9	16.8	A″	1438.0	4.7	Bu	1421.3	84.6	A	1455.2	22.0	1454.9, 1457.9	7, 2
Ag	1453.0	0	A′	1453.6	6	Ag	1428.9	0	A	1461.3	0.004	1471.1	3
Au	1591.1	427	A″	1591.6	12.3	Bg	1585.9	0	B	1581.7	383.1	1567.6	60
Bg	1593.3	0	A″	1592.3	384.9	Au	1588.1	369	A	1583.1	32.4	1571.5, 1571.4	88, 100
Au	2908.7	22.2	A″	2912.7	9.4	Au	2972.8	7	B	2940.7	17.3	2857.2	1
Ag	2910.3	0	A′	2914.4	29.2	Ag	2976.8	0	A	2945.8	1.7	2874.9, 2883.4	1, 0.5
Bg	2920.6	0	A″	2980.0	3.9	Bg	2984.2	0	B	2958.0	5.5	2891.4	0.6
Bu	2922.6	93.4	A′	2984.5	34.6	Bu	2989.2	40.1	A	2961.3	47.4	2965.3, 2967.4	2, 2
Au	3062.7	0.89	A″	3058.4	0.85	Bg	3070.9	0	B	3009.9	12.6		
Bg	3063.0	8.4	A′	3058.5	4.3	Ag	3071.4	1.5	A	3011.3	11.5	3025.3	12
Bu	3063.1	0	A″	3075.1	0.35	Au	3071.7	0	B	3050.6	11.3		
Ag	3063.2	0	A′	3075.3	0.98	Bu	3072.0	2	A	3051.1	0.2		

structures of p-DNP using thermodynamic calculations to test the validity of the percentages obtained from the observed vibrational patterns. The free energy of each of the conformers was computed using Gaussian 98 with a temperature of 358 K, which is the maximum temperature used in the experimental Knudsen beam. The ea conformer is predicted by both of the DFT methods to have the lowest value of the free energy. The free energy of each of the conformers relative to that of the ea conformer (denoted as $\Delta G°$) is given in Table 1. The relative populations of the conformers at 358 K are readily computed from the free energy differences and are listed in Table 1. The predicted populations are generally in good agreement for both DFT methods and with the populations derived from fitting the experimental spectrum. In particular, both the B3LYP and BP86 methods predict that due to entropy effects the ea conformer will have the largest population, which is consistent with results obtained independently using experimental data as described above. The B3LYP predicts that the population of the ee conformer is only slightly smaller than that of the ea conformer which is in excellent agreement with the 4% difference in the populations derived from the fit. The BP86 calculations predict a larger difference between the populations of the ea and ee conformers than is derived from the fitting procedure but there is still qualitative agreement with the population from the experimental spectrum given the errors in experimentally identifying the distribution of the conformers. Both DFT methods predict that the twisted-boat conformer is present in

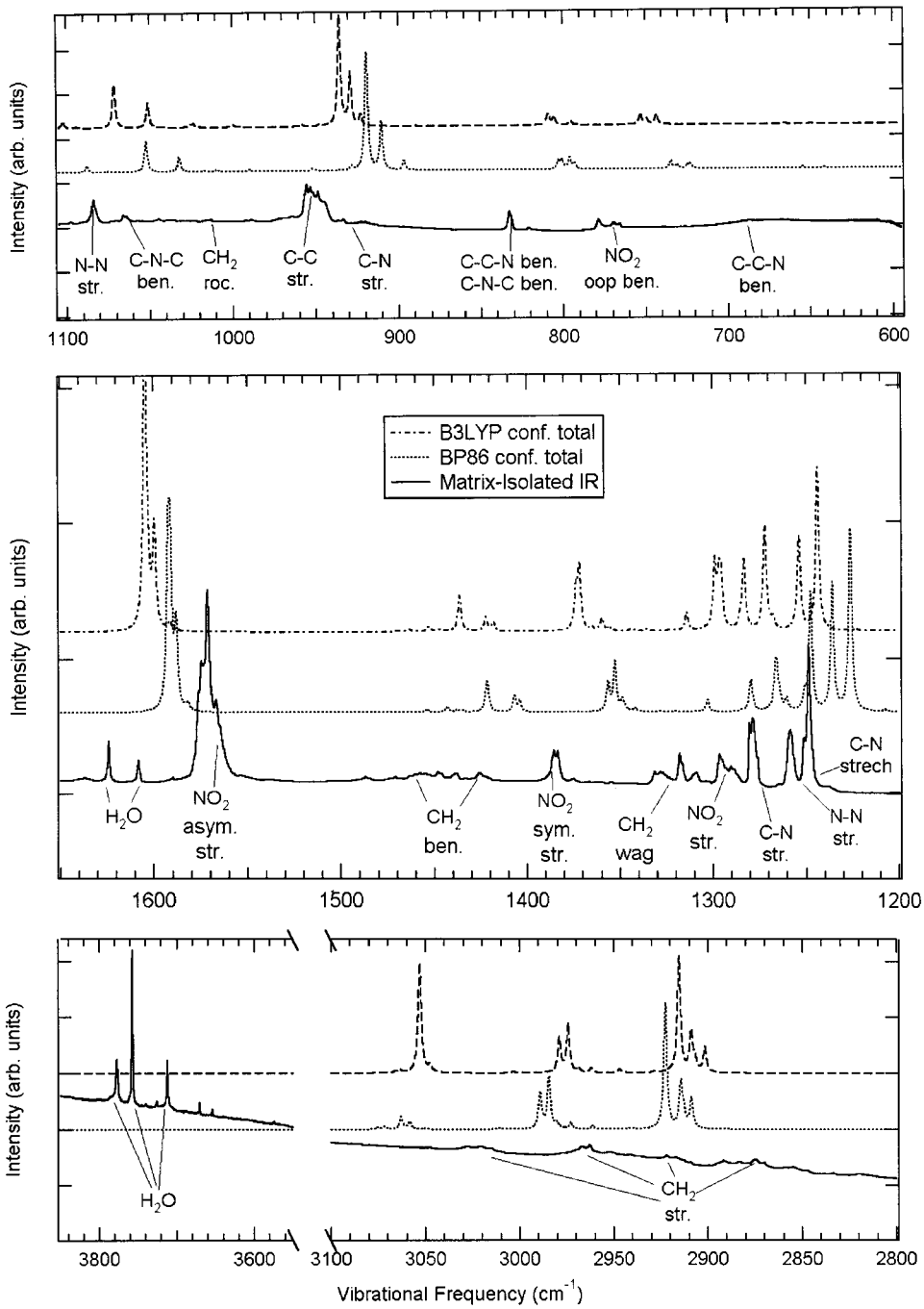

Figure 4. Observed matrix-isolated spectra and the simulated "weighted-sum" spectra with frequencies assigned to vibrational modes. The abbreviation "str" is used to indicate a stretching mode and the abbreviation "ben" is used to indicate a bending mode.

the spectrum as a minor contribution, as shown by the experimental data fit.

Comparing the spectra in Figure 4 makes it easier to relate the calculated vibrational modes to the experimental peaks. The next-to-the last column in Table 3 shows assigned experimental frequencies along the rows corresponding to the calculated modes. The final column in Table 2 shows relative intensities of the peaks in the experimental spectrum. Unfortunately, due to limitations on the accuracy of all calculations and because p-DNP naturally remains as a mixture of conformers from which we obtained our experimental data, it is impossible to exactly match each observed peak to a unique calculated vibration of a single conformer. (Unique assignments would require matrix-isolated IR spectra of individual conformers, a nearly impossible task considering the very low energy barriers to transition between conformers). Therefore, the experimental data has been assigned to features with multiple peaks, or to "blocks" of modes within narrow frequency ranges. In the last two columns of Table 3, horizontal lines separate these features or "blocks". However, it must be noted that all peaks in the matrix-isolated spectra have been assigned and that only 3−4 peaks of very low intensity are unassigned to a known vibrational mode. These peaks are too weak to be visibly discernible in plots of the IR spectra as in Figure 4, and therefore have not been listed here. We considered possible impurities, and found water to be the only contaminant of significant intensity. Other impurities that are part of the synthesis process of p-DNP or decomposition products of p-DNP, such as the nitroso derivative of the parent piperazine molecule would have stretching vibrations spectrally resolved from the p-DNP spectra. No additional vibrational

TABLE 4: Calculated and Observed Bond Lengths and Angles Compared

		B3LYP calculations							BP86 calculations						
		chair form					twist-boat form		chair form					twist-boat form	
coordinate	XRD expt value	ee	e*e TS	ea	aa* TS	aa	Tw* TS	ee	ee	e*e TS	ea	aa* TS	aa	Tw* TS	ee
R−N1−C2	1.454	1.465	1.467	1.468	1.459	1.470	1.465	1.465	1.468	1.469	1.470	1.459	1.472	1.469	1.471
R−C2−C4	1.514	1.527	1.532	1.533	1.538	1.538	1.555	1.529	1.534	1.539	1.539	1.544	1.545	1.561	1.534
R−C4−N6		1.465	1.455	1.465	1.468	1.470	1.464	1.464	1.468	1.457	1.469	1.471	1.472	1.467	1.468
R−N1−N7	1.370	1.398	1.400	1.399	1.377	1.402	1.374	1.379	1.420	1.422	1.421	1.398	1.426	1.395	1.404
R−N6−N8		1.398	1.377	1.403	1.402	1.402	1.383	1.379	1.420	1.399	1.428	1.426	1.426	1.401	1.404
R−C2−H2e	0.970	1.088	1.089	1.089	1.088	1.088	1.094	1.093	1.098	1.098	1.099	1.099	1.098	1.104	1.102
R−C2−H2a	0.970	1.100	1.100	1.100	1.098	1.094	1.094	1.097	1.109	1.110	1.110	1.108	1.104	1.103	1.107
R−C4−H4e		1.088	1.088	1.088	1.088	1.088	1.091	1.089	1.098	1.098	1.098	1.098	1.098	1.101	1.100
R−C4−H4a		1.100	1.098	1.094	1.094	1.094	1.096	1.096	1.109	1.107	1.103	1.104	1.104	1.106	1.105
R−N7−O7a	1.220	1.228	1.228	1.228	1.232	1.229	1.233	1.232	1.240	1.240	1.240	1.243	1.241	1.245	1.243
R−N8−O8a		1.228	1.231	1.228	1.229	1.229	1.231	1.231	1.240	1.243	1.240	1.241	1.241	1.243	1.243
A−C2−N1−C3	115.4	115.6	116.1	116.7	118.7	114.7	124.5	120.2	115.5	115.7	116.3	119.0	114.9	124.2	119.5
A−N1−C2−C4	109.4	109.1	108.8	108.8	109.5	110.6	115.2	108.6	108.8	108.5	108.5	109.5	110.9	115.0	108.4
A−C2−C4−N6		109.1	110.2	111.7	111.1	110.6	114.3	110.9	108.8	110.0	111.8	111.3	110.9	114.3	111.3
A−C4−N6−C5		115.6	117.9	113.8	114.5	114.7	121.1	120.2	115.5	118.4	114.1	114.7	114.9	121.8	119.5
A−C2−N1−N7	115.2	115.8	115.8	115.6	120.5	115.7	115.6	116.5	115.7	115.8	115.6	120.5	115.3	115.4	115.5
A−C5−N6−N8		115.8	121.0	116.1	116.0	115.7	117.6	116.5	115.7	120.7	115.6	115.6	115.3	117.6	115.5
A−N1−C2−H2e	109.8	108.6	108.5	108.5	108.3	108.8	108.4	109.4	108.3	108.2	108.2	107.8	108.4	108.6	109.5
A−N1−C2−H2a	109.8	110.5	110.5	110.8	109.1	106.7	108.2	110.6	110.7	110.6	110.9	109.4	106.8	108.1	110.5
A−N6−C4−H4e		108.6	108.4	108.9	108.8	108.8	107.7	107.7	108.3	107.9	108.4	108.3	108.4	107.7	107.0
A−N6−C4−H4a		110.5	108.8	106.4	106.4	106.7	109.5	109.7	110.7	109.2	106.5	106.5	106.8	109.4	109.5
A−N1−N7−O7a	116.8	116.9	116.9	116.9	117.1	117.1	116.5	115.9	116.6	116.6	116.6	116.8	116.8	116.0	115.4
A−N6−N8−O8a		116.9	117.1	117.0	117.0	117.1	116.2	117.8	116.6	116.8	116.7	116.7	116.8	115.8	117.7
D(C4−C2−N1−C3)	−56.1	−56.6	−57.1	−54.5	−51.2	−54.0	−4.3	23.6	−57.4	−58.5	−56.0	−51.3	−53.2	−6.6	22.7
D(N6−C4−C2−N1)	52.6	52.9	50.4	51.7	49.7	51.8	−5.3	−55.1	53.4	50.6	51.9	49.3	51.1	−5.8	−55.9
D(C5−N6−C4−C2)		−56.6	−52.2	−54.6	−55.0	−54.0	−21.5	31.5	−57.4	−51.5	−53.4	−54.1	−53.2	−19.1	32.8
D(N7−N1−C2−C4)	165.8	163.4	162.2	164.6	123.7	84.5	−166.1	179.4	163.0	161.3	163.7		125.8	84.6	−166.1
D(N8−N6−C4−C2)		163.4	122.5	84.0	84.2	84.5	−173.2	−123.7	163.0	124.5	84.3	84.3	84.6	−171.8	−116.5
D(N6−C4−C2−H2e)	173.2	171.8	169.3	170.6	169.5	173.1	−127.3	−174.7	172.0	169.1	170.6	168.6	172.0	−128.1	−175.7
D(N6−C4−C2−H2a)	−67.9	−68.6	−70.8	−69.9	−70.1	−66.0	116.9	66.6	−68.0	−70.7	−69.7	−70.8	−66.9	116.1	65.6
D(N1−C2−C4−H4e)		171.8	170.3	173.2	171.0	173.1	115.8	−174.3	172.0	169.8	172.8	170.1	172.0	115.3	−174.6
D(N1−C2−C4−H4a)		−68.6	−69.4	−66.3	−68.0	−66.0	−128.0	66.7	−68.0	−69.6	−66.4	−68.7	−66.9	−128.7	66.1
D(O8a−N8−N6−C5)	161.2	−161.2	177.5	160.3	160.8	160.5	−166.7	−171.5	−161.2	178.2	160.4	160.9	160.6	−167.3	−168.6
D(O8b−N8−N6−C5)	22.9	21.3	−3.0	−22.7	−22.2	−22.4	14.8	10.2	21.7	−2.3	−23.3	−22.8	−23.0	14.4	13.7
D(O7a−N7−N1−C2)		−21.3	−20.8	−20.5	2.7	22.4	−10.7	10.2	−21.7	−21.4	−21.2	1.6	23.0	−11.2	13.7
D(O7b−N7−N1−C2)	161.2	161.7	162.0	−177.6	−160.5	170.3	−171.5	161.2	161.6	161.8	−178.6	−160.0	170.1	−168.6	
D(C5−N6−C4−N8)	138.2	140.0	−174.7	−138.6	−139.2	−138.5	151.7	155.2	139.7	−176.0	−137.7	−138.5	−137.8	152.7	149.4
D(C3−N1−C2−N7)		140.0	140.8	141.0	−174.9	−138.5	161.8	−155.8	139.7	140.3	140.3	−177.1	−137.8	159.6	−150.1

frequencies are observed within the experimental limitations. If any other impurities are present, it is estimated that these species are less than 1 ppm because all the main IR peaks have been identified and assigned. Therefore, the three chair conformers of p-DNP have been identified. Finally, the twisted-boat conformer has been calculated to exist under the conditions of the experiment. Since the twisted-boat conformer concentration is very small, definitive assignment of this species is not possible at this time. However, spectral evaluation of the observed vibrational frequencies indicates its presence.

Table 4 presents calculated and experimentally obtained structural information. Interestingly, only the ee chair conformer is observed via X-ray diffraction of solid DNP.[18] This is possibly due to packing energies associated with packing multiple conformers making the ee chair conformer the favored structure of the more dense solid form. Values in the "expt" column of Table 4 are averages of bond length and bond-angle values observed from X-ray diffraction. Solid-state effects cause nonequivalence for many bond lengths and angles that are equivalent for isolated gas-phase molecules. Differences caused by solid state effects and errors in the theoretical methods cannot be easily evaluated. The calculated results are in qualitative agreement with experimental values for most angles and bond lengths. The positions of hydrogen atoms are difficult to determine via X-ray diffraction because hydrogen has a very low molecular weight. Therefore, since bond lengths between H atoms and other atoms cannot be easily experimentally evaluated, comparison with theory is difficult. However, the ring angles and ring bond lengths can be estimated from diffraction.

Because the three chair conformers are lower in energy than the twist-boat conformer and are the major species seen in the experimental IR spectrum, we begin the discussion of the structural properties for p-DNP by focusing on the chair conformers and their transition states. As would be expected for conformers that differ only in the positions of the NO_2 groups, there are only relatively minor differences in bond lengths between the ring atoms among the chair conformers. However, significant differences in the ring angles are seen, particularly for the transition state structures. The rings of the three chair conformers considered are described by three different C−N−N and C−N−C angles. The C−N−C angle increases by 4° as the NO_2 group moves from the axial position to the aa* transition state (TS) leading to the equatorial position. Similarly, the C−N−N angles increase by about 5°, to slightly more than 120°, at the aa* TS. For this aa* TS the C−N−C bonds and NO_2 groups are approximately coplanar. When the NO_2 group moves from aa* TS to the ae position, the C−N−C angle decreases by about 2°.

The N−N bond length decreases by about 0.02 Å in the transition states between the axial and equatorial positions for the chair structures. This is accompanied by an increase in the N−O bond lengths but this change is on the order of 0.003 Å or an order of magnitude smaller. These bond length changes, along with the planarity of the C−N−C and NO_2 groups are consistent with the development of a small pi bonding contribution between the two nitrogen atoms. The N−N bond lengths of the three chair conformers are comparable but slightly longer in the axial position than the equatorial. The N−N−O bond angles, however, remain almost unchanged from around 117° for each of the five chair structures studied.

The bonding angles of the H atoms attached to the ring carbons do change in the chair conformers. The $N-C-H_{ax}$ decreases by 4° as the NO_2 group moves from the equatorial to the axial position. In contrast, the $N-C-H_{eq}$ angle is relatively constant for the three geometries. The behavior of these bond angles is correlated to the vibrational frequencies of the CH stretch modes. The increase in the $N-C-H_{ax}$ bond angle is accompanied by an increase in the vibrational frequency of the CH stretching modes involving the axial hydrogen atoms. In contrast, the frequencies of the stretching modes involving the equatorial H atoms are relatively unchanged. The $C-C-H_{eq}$ angle increases by 1.5° between the eq−eq and ax−ax geometries, though the $C-C-H_{ax}$ angle is relatively constant.

Significant differences are seen in the structural features of the twisted-boat conformer. The C−N−C angle for the twisted-boat conformer, at 120.2°, is larger than the value obtained for any of the chair conformers. This angle increases by 4° for the twisted-boat TS, which increases the ring strain but acts to reduce the torsional strain that is induced as neighboring CH_2 groups move into an eclipsed configuration. The N−N bonds in the twisted-boat conformer are shorter than those for the chair conformers by 0.02 Å but the N−O bonds are slightly longer. Note that the N−N and N−O bond lengths are comparable to those for the aa* chair transition state structure, which also has the largest C−N−C angle. Another point of similarity between the twisted-boat conformer and the aa* chair transition state structure is that the C−N−C and NO_2 groups are almost coplanar.

Conclusions

The conformers of p-DNP have been investigated theoretically and experimentally. The relative stability and structure of the conformers of p-DNP were determined using GAUSSIAN 98 with the B3LYP and BP86 density functional methods. These calculations indicate that the total energies of the conformers are comparable (within 0.5 kcal/mol) with the equatorial-equatorial conformer being the most stable. Infrared spectra of matrix-isolated p-DNP were obtained at 11 K. The three p-DNP chair conformers (ee, ea, aa) have been identified. Comparing the calculated vibrational frequencies to the experimentally obtained spectrum, the observed spectrum was identified as being composed primarily of the three chair conformers with a few percent of the twisted-boat conformer. The distribution of the conformers observed is estimated to be 0.9:1:0.6:0.05. Computed vibrational frequencies were used to assign vibrational mode symmetries to the observed frequencies. Calculated bond lengths and angles were compared to those found in the solid-state p-DNP structure and most of the calculated values are in qualitative agreement with the experimental data.

References and Notes

(1) Oyumi, Y.; Rheingold, A. L.; Brill, T. B. *J. Phys. Chem.* **1986**, *90*, 4686−4690.
(2) Brill, T. B.; Oyumi, Y. *J. Phys. Chem.* **1986**, *90*, 6848−6853.
(3) Oxley, J. C.; Kooh, A. B.; Szekeres, R.; Zheng, W. *J. Phys. Chem.* **1994**, *98*, 7004−7008.
(4) Zeman, S. *Thermochim. Acta* **1997**, *302*, 11−16.
(5) Zeman, S.; Dimun, M.; Trucklik, S. *Thermochim. Acta* **1984**, *78*, 181−209.
(6) Politzer, P.; Murray, J. S.; Lane, P.; Sjorberg, P.; Adolph, H. G. *Chem. Phys. Letts.* **1991**, *181*, 78−82.
(7) Murray, J. S.; Redfern, P. C.; Lane, P.; Politzer, P. *J. Mol. Struct. (THEOCHEM)* **1990**, *207*, 177−191.
(8) Murray, J. S.; Redfern, P. C.; Seminario, J. M.; Politzer, P. *J. Phys. Chem.* **1990**, *94*, 2320−2323.
(9) George, M. V.; Wright, G. F. *J. Am. Chem. Soc.* **1958**, *80*, 1200−1204.
(10) Calderbank, K. E.; Pierens, R. K. *J. Chem. Soc., Perkins Trans. 2* **1979**, 869−871.
(11) Becke, A. D. *Phys. Rev. A* **1988**, *38*, 3098.
(12) Perdew, J. P. *Phys. Rev. B* **1986**, *33*, 8822.

(13) Becke, A. D. *J. Chem. Phys.* **1993**, *98*, 5648.
(14) Lee, C.; Yang, W.; Parr, R. G. *Phys. Rev. B* **1988**, *37*, 785.
(15) Frisch, M. J.; Trucks, G. W.; Schlegel, H. B.; Scuseria, G. E.; Robb, M. A.; Cheeseman, J. R.; Zakrzewski, V. G.; Montgomery, J. A., Jr.; Stratmann, R. E.; Burant, J. C.; Dapprich, S.; Millam, J. M.; Daniels, A. D.; Kudin, K. N.; Strain, M. C.; Farkas, O.; Tomasi, J.; Barone, V.; Cossi, M.; Cammi, R.; Mennucci, B.; Pomelli, C.; Adamo, C.; Clifford, S.; Ochterski, J.; Petersson, G. A.; Ayala, P. Y.; Cui, Q.; Morokuma, K.; Malick, D. K.; Rabuck, A. D.; Raghavachari, K.; Foresman, J. B.; Cioslowski, J.; Ortiz, J. V.; Stefanov, B. B.; Liu, G.; Liashenko, A.; Piskorz, P.; Komaromi, I.; Gomperts, R.; Martin, R. L.; Fox, D. J.; Keith, T.; Al-Laham, M. A.; Peng, C. Y.; Nanayakkara, A.; Gonzalez, C.; Challacombe, M.; Gill, P. M. W.; Johnson, B.; Chen, W.; Wong, M. W.; Andres, J. L.; Gonzalez, C.; Head-Gordon, M.; Replogle, E. S.; Pople, J. A. *Gaussian 98*, Revision A.6; Gaussian, Inc.: Pittsburgh, PA, 1998.
(16) Ditchfield, R.; Hehre, W. J.; Pople, J. A. *J. Chem. Phys.* **1971**, *54*, 724. Hehre, W. J.; Ditchfield, R.; Pople, J. A. *J. Chem. Phys.* **1972**, *56*, 2257.
(17) Scott, A. P.; Radom, L. *J. Phys. Chem.* **1996**, *100*, 16502−16513.
(18) Gillardi, R. N. Private Communication, Coordinates are: CCDC 136083, at the Cambridge Crystallographic Database Centre, 12 Union Rd., Cambridge, CB2 1EZ, U.K.